AFRL-SN-RS-TR-1998-190
In-House Report
December 1998

PHOTOREFRACTIVES FOR OPTICAL SIGNAL PROCESSING
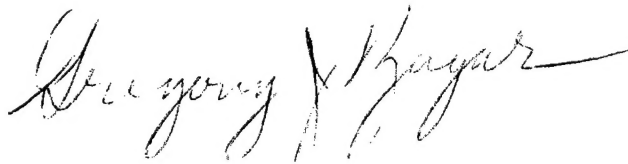
George A. Brost

19981229 011

**AIR FORCE RESEARCH LABORATORY
SENSORS DIRECTORATE
ROME RESEARCH SITE
ROME, NEW YORK**

This report has been reviewed by the Air Force Research Laboratory, Information Directorate, Public Affairs Office (IFOIPA) and is releasable to the National Technical Information Service (NTIS). At NTIS it will be releasable to the general public, including foreign nations.

AFRL-SN-RS-TR-1998-190 has been reviewed and is approved for publication.

APPROVED:

GREGORY J. ZAGAR
Chief, RF Photonics Branch
Sensors Directorate

FOR THE DIRECTOR:

ROBERT G. POLCE
Acting Chief, Rome Operations Office
Sensors Directorate

If your address has changed or if you wish to be removed from the Air Force Research Laboratory Rome Research Site mailing list, or if the addressee is no longer employed by your organization, please notify AFRL/SNDR, 25 Electronic Pky, Rome, NY 13441-4515. This will assist us in maintaining a current mailing list.

Do not return copies of this report unless contractual obligations or notices on a specific document require that it be returned.

REPORT DOCUMENTATION PAGE

Public reporting burden for this collection of information is estimated to average 1 hour per response, including the time for reviewing instructions, searching existing data sources, gathering and maintaining the data needed, and completing and reviewing the collection of information. Send comments regarding this burden estimate or any other aspect of this collection of information, including suggestions for reducing this burden, to Washington Headquarters Services, Directorate for Information Operations and Reports, 1215 Jefferson Davis Highway, Suite 1204, Arlington, VA 22202-4302, and to the Office of Management and Budget, Paperwork Reduction Project (0704-0188), Washington, DC 20503.

1. AGENCY USE ONLY (Leave blank)	2. REPORT DATE	3. REPORT TYPE AND DATES COVERED
	December 1998	In House, Oct 95 - Jun 98

4. TITLE AND SUBTITLE

PHOTOREFRACTIVES FOR OPTICAL SIGNAL PROCESSING

5. FUNDING NUMBERS

PE - 62702F
PR - 4600
TA - P1
WU- 18

6. AUTHOR(S)

George A. Brost

7. PERFORMING ORGANIZATION NAME(S) AND ADDRESS(ES)

Air Force Research Laboratory/SNDR
25 Electronic Pky
Rome, NY 13441-4515

8. PERFORMING ORGANIZATION REPORT NUMBER

AFRL-SN-RS-TR-1998-190

9. SPONSORING/MONITORING AGENCY NAME(S) AND ADDRESS(ES)

Air Force Research Laboratory/SNDR
25 Electronic Pky
Rome, NY 13441-4515

10. SPONSORING/MONITORING AGENCY REPORT NUMBER

AFRL-SN-RS-TR-1998-190

11. SUPPLEMENTARY NOTES

Air Force Research Laboratory Project Engineer: George A. Brost/SNDR/(315) 330-7669

12a. DISTRIBUTION AVAILABILITY STATEMENT

APPROVED FOR PUBLIC RELEASE; DISTRIBUTION UNLIMITED.

12b. DISTRIBUTION CODE

13. ABSTRACT (Maximum 200 words)

Photorefractive recording dynamics of two-beam coupling were investigated theoretically and experimentally. The interaction of beams with slightly different frequencies were studied in semi-insulating semiconductors. The influences of bulk absorption, Gaussian beam profiles and experimental geometry on the temporal response were analyzed. These effects were shown to narrow the response bandwidth. Enhancement of the steady-state photorefractive response in tin hypothiodiphosphate (Sn2P2P6) by use of the moving grating technique, without an applied electric field, was demonstrated.

14. SUBJECT TERMS

photorefractive, bulk absorption, Gaussian beam profiles, experimental geometry, tin hypothiodiphosphate (Sn2P2P6)

15. NUMBER OF PAGES

52

16. PRICE CODE

17. SECURITY CLASSIFICATION OF REPORT	18. SECURITY CLASSIFICATION OF THIS PAGE	19. SECURITY CLASSIFICATION OF ABSTRACT	20. LIMITATION OF ABSTRACT
UNCLASSIFIED	UNCLASSIFIED	UNCLASSIFIED	UL

TABLE OF CONTENTS

LIST OF FIGURES

1. INTRODUCTION

The photo-induced refractive index change in electro-optic materials, known as the photorefractive effect, exhibits unique capabilities. Dynamic holographic phase gratings can be generated in these materials with low power laser beams. The photorefractive nonlinear optical effect has many applications in optical signal processing. An understanding of the photorefractive characteristics is important to the successful utilization of these nonlinear effects. In this paper we report on research on photorefractive materials and effects.

Section 2 describes investigation of the temporal response of semiconductor photorefractives. Here the influence of beam size and geometry on the gain spectra is studied. In Section 3 we report on a new photorefractive material for the near infrared, tin hypothiodophosphate.

2. GAIN SPECTRA OF PHOTOREFRACTIVE SEMICONDUCTORS.
2.1. INTRODUCTION

Measurement of the temporal response of two-beam coupling in photorefractive materials is important for determination of material parameters and for device characterization. However, there are a number of experimental and material factors that can strongly influence such measurements. These factors include bulk absorption, beam intensity profiles, coupling geometry, coupling strength, modulation depth, dark current, and pump depletion. Even under conditions in which only absorption appears to be a factor, the bandwidth of the material can be drastically different than that predicted by the standard photorefractive theory.

1

In fast photorefractive materials, such as the II-VI and III-V semiconductors, it is often convenient to measure the temporal response in the frequency domain rather than the time domain. This approach avoids the requirement of fast shutters and detectors, and has the advantage that measurements in the frequency domain are carried out entirely in the steady state regime. In addition, for purposes of accounting for the influences on the temporal response mentioned above, work in the frequency domain is particularly convenient since modelling is often more readily done there.

In the diffusion regime, the standard solution of the material equations for a material with one kind of photorefractive trap predicts that the time dependence of the gain coefficient is given by[1]

$$\Gamma = \Gamma_0 (1 - exp(-t/\tau)), \qquad\qquad 2.1$$

where Γ_0 is the steady state gain coefficient and τ is the photorefractive time constant. In the frequency domain, the two-beam coupling gain spectra for moving gratings is given by[2]

$$\Gamma = \Gamma_0 / (1 + \Omega^2 \tau^2), \qquad\qquad 2.2$$

where Ω is the angular frequency detuning between the pump and signal beams. Eq. (2) is a simple Lorentzian function centered at $\Omega = 0$ Hz. Derivation of Eqs. (2.1) and (2.2) assumes negligible contributions from the factors mentioned above .In particular, it assumes a lossless material and plane wave illumination. In practice, these conditions

2

cannot be met. The photorefractive response time is dependent on intensity and is therefore position dependent in the material.

The effect of absorption on the photorefractive response was investigated in references 3-5. Dai *et al.*[3] and Delaye *et al.*[4] showed that the bandwidth of the response narrows for a lossy material. Hermanns *et al.*[5] derived the transfer function in the presence of absorption and the absence of pump depletion. The problem of two-beam coupling with focussed Gaussian beams in planar waveguides was analyzed by Fluck *et al.*[6] In this case the interaction length was determined by the beam profile, rather than the thickness of the material. They found that the transverse intensity distribution of the Gaussian beams must be taken into account in evaluation of the gain and that the time response can differ from that predicted by plane wave theory. Boutsikaris and Davidson[7] dealt with the problem of transient two-beam coupling with non-plane-wave beams in a lossless medium.

Part of the reason that the problem of two-beam coupling including simultaneous absorption and non-plane-wave beams had not been widely treated may be due partly to the fact that in the absence of dark current or beam depletion effects, the steady-state gain is relatively insensitive to total intensity. The temporal response, on the other hand, is very sensitive to the volume distribution of the intensity in the material. Optical absorption and beam geometries both are important factors which influence the gain spectra of semiconductors. For a given input light intensity the optical absorption determines the upper limit of the bandwidth. For typical experimental configurations in bulk photorefractives, in which the beams are not strongly focussed, the beam profiles do

not strongly influence the steady state, degenerate two-beam coupling gain, since the interaction length is determined by the material thickness. For focussed or small diameter beams, issues of beam depletion and dark intensity come into play and the interaction length may be determined by the beam profiles themselves.[6]

In this section, we study the influence of a spatially dependent light intensity distribution on the gain spectra of the photorefractive. It is assumed here that dark current, large modulation, and pump depletion are not present, and that the gain is in the small signal regime. We present a theoretical analysis which elucidates the effects of optical absorption and Gaussian beam profiles. We also present experimental results of gain spectra and temporal response measured in photorefractive semiconductors. It is found that the frequency response can significantly depart from the Lorentzian shape of Eq. (2.1). We use a simple method of eliminating these influences for the purpose of measuring the material photorefractive time constant.

2.2 THEORY

2.2.1 Absorption

In this section we consider the effect of optical absorption on the gain spectra. We assume that the signal beam intensity is much smaller than the pump beam intensity, and the pump beam provides uniform illumination distribution in the transverse direction but falls off exponentially with distance according to Beer's Law, $I(z) = I_0 \exp(-\alpha z)$. We also

4

assume that the photorefractive response time is inversely proportional to some power q of the light intensity, so that the position dependent response time is given by

$$\tau(z) = \tau_0(I_0/I(z))^q = \tau_0 \exp(q\alpha z),$$

2.3

where τ_0 is the photorefractive time constant at intensity I_0, at the front of the crystal. The integral gain coefficient for moving gratings is then given by

$$\Gamma = \frac{1}{L}\int_0^L \frac{\Gamma_0}{1+\Omega^2\tau^2(z)}dz ,$$

2.4

where L is the interaction length. After substitution for $\tau(z)$ and integration the final expression for the gain spectrum becomes

$$\Gamma = \Gamma_0\left[1+\frac{1}{2q\alpha L}\ln\left(\frac{1+\Omega^2\tau_0^2}{1+\Omega^2\tau_0^2\exp(2q\alpha L)}\right)\right].$$

2.5

This result agrees with the transfer function derived by Hermanns *et al*[5] for $q = 1$. Fig. 2.1 demonstrates the effect of absorption on the gain spectra. Here we plot the gain coefficient as a function of the normalized frequency detuning for three different values of αL with $q = 1$; (a) $\alpha=0$, (b) $\alpha L = 0.72$, and (c) $\alpha L = 5$. Curve a is the single

5

Lorentzian profile given by Eq. (2.2) for no absorption. Curve *b* reflects an αL for typical crystal parameters. In this case the gain profile can still be characterized as single Lorentzian, but narrower than for no absorption. This result shows that the effect of absorption for most crystals is to increase the exponential time constant, in this case by about a 50%. Curve *c* demonstrates the effect of very large absorption. In this case the gain profile is much narrower (by about a factor of ten) than the no absorption case. It can no longer be characterized as a single Lorentzian. In fact, it is more accurately described as the sum of two Lorentzians.
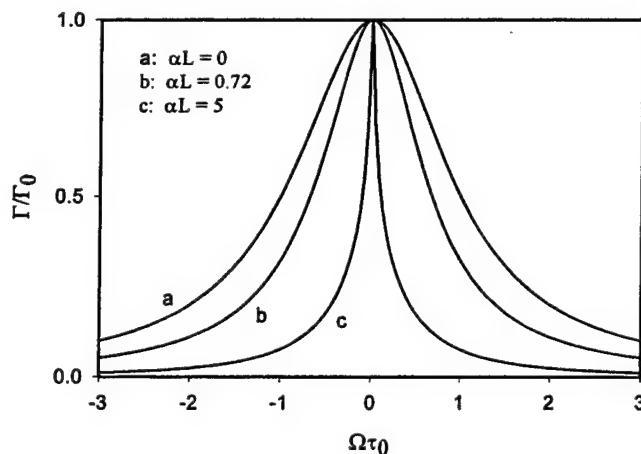

Figure 2.1 Gain spectra for three values of αL.

2.2 .2 Gaussian beam profiles.

We now consider the more general case of finite beam sizes. The geometry is as shown in Fig. 2.2. The signal beam I_S and pump beam I_p cross inside the crystal of thickness d at an angle of 2θ. The intensity profiles of the signal and pump beams are assumed to be Gaussian, and are given by

$$I_S(x,y,z) = I_{S0} \exp\left(\frac{-2(x^2+y^2)}{\omega_S^2}\right) \exp(-\alpha z)$$

2.6

and

$$I_S(x',y',z') = I_{S0} \exp\left(\frac{-2(x'^2+y'^2)}{\omega_P^2}\right) \exp(-\alpha z'),$$

2.7

where $2\omega_S$ and $2\omega_P$ are the $1/e^2$ intensity diameters of the signal and pump beams, respectively. As before, we assume that the pump beam intensity is much larger than the signal beam intensity, so that $\tau(I)$ is determined by I_p. The gain coefficient is calculated by integrating the differential gain coefficient over the volume of the signal beam. After a coordinate transformation from the primed to the unprimed coordinates, and taking the origin to be where the beams cross, the gain coefficient is given by

7
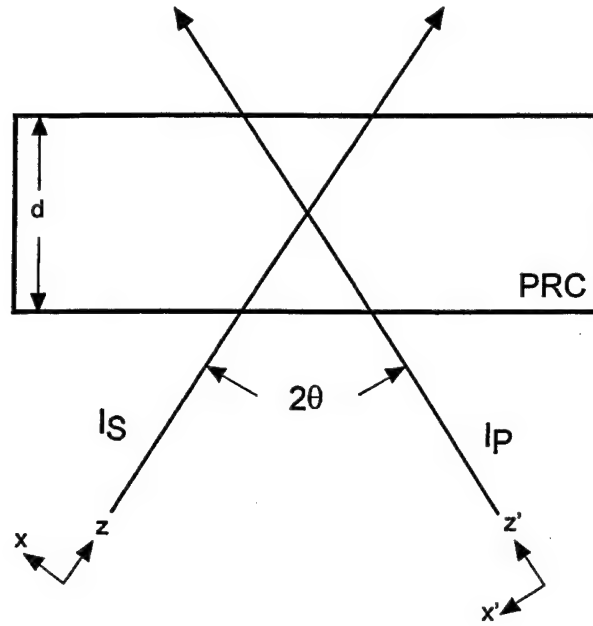
Fig. 2.2. Schematic of beam coupling intereaction.

$$\Gamma = \frac{\Gamma_0 2\cos(\theta)}{\pi \omega_S^2 d} \int_{-\frac{\xi d}{\cos(\theta)}}^{\frac{(1-\xi)d}{\cos(\theta)}} \int_{-\infty}^{\infty} \int_{-\infty}^{\infty} \frac{e^{\left(\frac{-2(x^2+y^2)}{\omega_s^2}\right)} dydxdz}{1+\Omega^2 \tau_0^2 e^{\left(2q\alpha\left[-\sin(2\theta)x+\cos(2\theta)y+\frac{\zeta d}{\cos(\theta)}\right]\right)} e^{\left(\frac{4[\cos(2\theta)x+\sin(2\theta)z]^2+4y^2}{\omega_p^2}\right)}}$$

$$2.8$$

Here the differential gain was weighted according to the Gaussian profile of the signal beam, d is the crystal thickness, and ξ is a parameter that indicates the location of the origin. The integral in Eq. (2.8) was evaluated numerically.

8

FIG 2.3. Calculated gain spectra for different crossing angles. Parameters were $q = 1$, $\alpha = 1.2$ cm^{-1}, $d = 0.6$ cm, $2\omega_s = 2$mm, $2\omega_p = 2$mm, $\xi = \frac{1}{2}$.
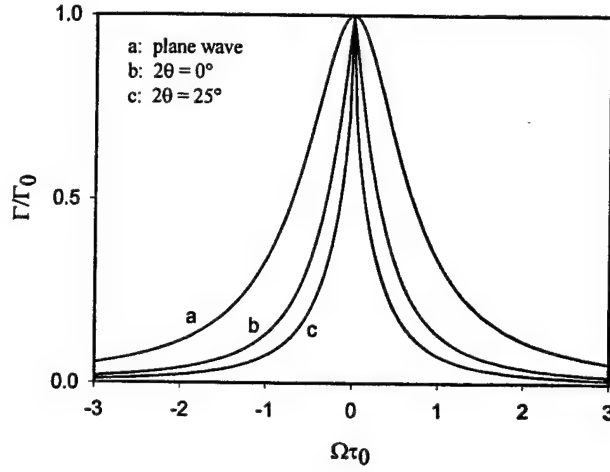
There are seven parameters that influence the gain coefficient in Eq. (2.8); q, α, d, ω_s, ω_p, θ, and ξ. It is not possible here to fully evaluate the effect of each parameter. We highlight some of the more important features. In the following analysis we let $q = 1$, $\alpha = 1.2$ cm^{-1}, $d = 0.6$ cm, and $2\omega_s = 2$ mm.

In Fig. 2.3 the calculated gain spectra are plotted for crossing angles of $2\theta = 0°$ and $25°$, with $2\omega_p = 2$ mm and the beams crossing in the center of the crystal ($\xi = \frac{1}{2}$). The gain calculated from Eq. (5) for plane waves is also shown for comparison (curve a). The position dependent intensity associated with the Gaussian beam profile causes a significant narrowing of the bandwidth as compared to that of the plane wave case; a factor of about five for $2\theta = 25°$. The resulting gain spectrum is similar to that of the plane wave, large absorption example in Fig. 1. Of course, the departure from Lorentzian shape is less pronounced for thin crystals.

The influence of the Gaussian beam profile can be minimized with an expanded pump beam. Fig. 2.4 shows the calculated gain for a crossing angle of $2\theta = 25°$, $\xi = \frac{1}{2}$, and $\omega_P = \omega_S$, $2\omega_S$, and $5\omega_S$. There is still appreciable narrowing of the gain spectrum for $\omega_P = 2\omega_S$, but the spectrum is not much different than the plane wave case for $\omega_P = 5\omega_S$.

In the previous examples the beams were assumed to cross at the center of the crystal. Fig. 2.5 shows the calculated gain spectra for different crossing locations, $\xi = 0, \frac{1}{2}$, and 1, corresponding to the front, center, and back of the crystal, with $\omega_P = 3\omega_S$ and a crossing angle of $2\theta = 25°$. Although the steady state gain in the degenerate case does not depend on ξ, the bandwidth does. The widest bandwidth is obtained when the beams cross at the center of the crystal.
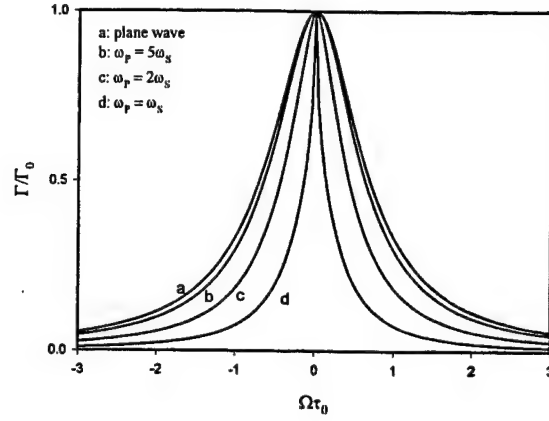
FIG 2. 4. Calculated gain spectra for different pump beam sizes. Parameters were $q = 1$, $\alpha = 1.2$ cm^{-1}, $d = 0.6$ cm, $2\omega_S = 2$mm, $2\theta = 25°$, $\xi = \frac{1}{2}$.
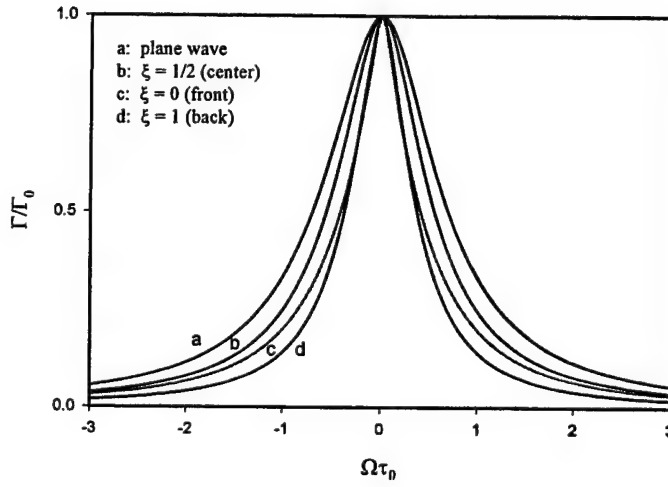

FIG 2.5. Calculated gain spectra for different beam crossing locations. Parameters were $q = 1$, $\alpha = 1.2$ cm^{-1}, $d = 0.6$ cm, $2\omega_S = 2$mm, $2\omega_P = 6$mm, $2\theta = 25°$.

2.2.3 Discussion.

With a nonuniform intensity distribution, the photorefractive time constant is position-dependent. The measured response is then a superposition of the response at all points in the crystal volume occupied by the signal beam. As the frequency is increased, the slower parts of the crystal, corresponding to lower total light intensity, fall off first in gain. At high frequencies only the fast parts of the crystal have significant gain. The net result is a faster fall-off of measured gain with frequency than is expected from the case of uniform intensity, that is, a narrowing of the system bandwidth. While bulk absorption causes the gain near the exit face of the crystal to decrease more rapidly with frequency than at the entrance face, the Gaussian intensity profile of the pump beam causes the gain to decrease with frequency nonuniformly in a direction approximately transverse to the signal beam. The gain spectra given by Eq. (2.8) predicts the photorefractive response in the presence of absorption and collimated Gaussian beams.

We comment here on some limits of applicability in using Eq. (2.8). The main limitation concerns the assumption that the pump beam intensity is significantly greater than the signal beam. This applies not just to the peak intensities, but throughout the volume of the signal beam. Equation (2.8) assumes that the time dependence is determined by the pump beam intensity alone, and not that of the signal beam. Also, this approach does not account for the effects of large modulation, beam depletion, or dark current which could occur in the Gaussian wings. Consequently, the limit of application depends upon the geometry of the problem. The examples presented here are valid for beam ratios

greater than 100. In the case of small beam diameters and thick crystals, the photorefractive interaction may occur far enough out in the wings of the pump beam that these assumptions are no longer valid. For these problems the numerical approach of Fluck *et al*[6] is more appropriate. Also, it should be noted that the results presented here are limited to beam coupling. The diffraction efficiency spectra may be different. This is because beam coupling gain is independent of modulation, while the diffraction efficiency is proportional to m^2. With Gaussian beams the modulation will be position dependent.

The analysis did not consider the effects of beam coupling on the time constant. Analysis of the photorefractive response that included the interaction of the optical field with the space charge field has shown a decreased bandwidth for materials with large ΓL, such as the ferroelectrics.[8,9] For semiconductors, the gain is sufficiently small that this effect is negligible.

A non-Lorentzian gain spectra may be obtained under certain experimental conditions, even when the pump beam diameter is much greater than the signal beam diameter. The nonlinearity of the photorefractive response is such that at large modulation the response becomes superlinear, but with a very slow temporal component.[10] A calculation of the gain spectra for different values of m is shown in Fig. 2.6. These results are solutions of the material equations and reflect the local response for plane waves. For $m < 0.6$ the response does not deviate much from the small m result of Eq. (2). For larger values of m, the space charge field is enhanced, but only for small frequency shifts due to the slow time component.

It should also be noted that deviations from the Lorentzian shape may occur, for reasons related not to the experimental conditions, but to the physics. An example is in the case of $Sn_2P_2S_6$,[11] where a dip in the gain occurs around 0 Hz. This dip points to the presence of a second grating of opposite sign. Similar deviations could happen in other photorefractive crystals, including semiconductors, where, for example, electron-hole competition is sometimes observed.
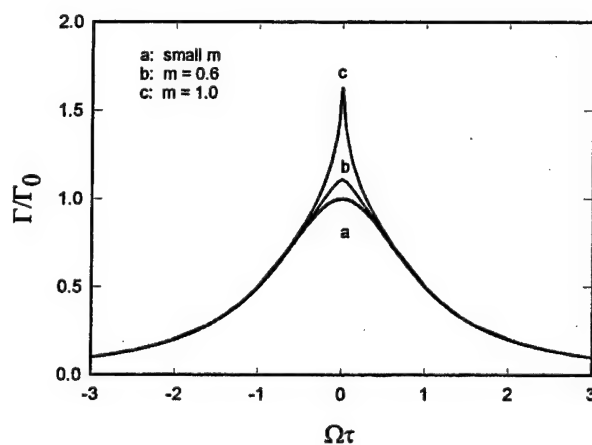
FIG 2.6. Calculated gain spectra for different values of modulation *m*.

2.3. EXPERIMENTAL RESULTS

In this section we present measured two-beam coupling frequency and time response data. As predicted in Section 2.2, it is found that the temporal response varies considerably with changes in Gaussian beam sizes and coupling geometry, and is influenced strongly by the bulk absorption of the material.

FIG 2.7. Configuration for the measurements of frequency and time response of two-beam coupling. M1, M2, M3, M4: mirrors; $\lambda/2$: half-wave plate; pol: linear polarizer; BS: beamsplitter; EOM: electro-optic phase modulator: BE: variable beam expander; S: mechanical shutter; PD: photodetector; ND: neutral density filters.

The experimental configuration for our measurements of two-beam coupling frequency and time response is shown in Fig. 2.7. The moving grating was produced in the photorefractive crystal by a linear phase modulation of on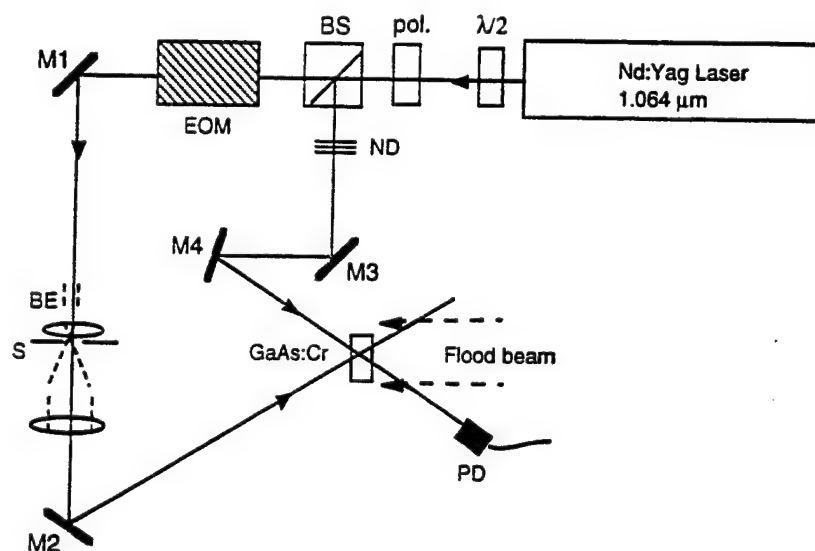e of the beams using an electro-optic phase modulator. In the frequency response measurements, the steady-state gain was measured as a function of the frequency, $f = \Omega / 2\pi$, of the ramp applied to the e-o modulator. The velocity of the grating is simply related to this frequency by $v_g = \Lambda \cdot f$, where Λ is the grating spatial period, since the ramp amplitude was adjusted for a 2π phase excursion.

The two-beam coupling measurements were performed at a wavelength of 1.06µm and a grating period of 0.7µm. The laser beams were incident on the $\left(1\bar{1}0\right)$ face of the GaAs:Cr crystal, the grating vector was oriented in the $\langle 001 \rangle$ direction, and the beams were s-polarized, i.e. along the $\langle 110 \rangle$ direction, in order to take advantage of the r_{41} electro-optic coefficient. The dimensions of the crystal, in the directions $\langle 110 \rangle \times \langle 100 \rangle \times \langle 1\bar{1}0 \rangle$, were 11x10x6.1 mm^3 and the measured absorption coefficient was 1.2 cm^{-1}.

Our two-beam coupling frequency and time response data for the GaAs:Cr sample, corresponding to various illumination conditions, are shown in Figs. 2.8-2.14. In what follows, we will describe the effects of these illumination conditions and of the material absorption on the temporal response of our sample.

(a)

Absorption model fit parameters:
(Eq. (5))

$\alpha = 7.86(0.24)$ cm^{-1}
$\tau_0 = 1.75(0.013)$ msec

Γ (cm^{-1})

f (Hz)

(b)

Gain

Fit parameters: (Eq. (9)):

$C = 0.356(0.0004)$
$\tau = 1.97(0.02)$ msec

Time (sec)

FIG 2.8. Temporal response of the GaAs:Cr sample. $1/e^2$ beam diameters: 2.0mm (pump) and 1.8mm (signal). Spatially averaged beam intensities are $I_{pump} = 1.55\ W/\ cm^2$ and $I_{signal} = 2.4\ mW/\ cm^2$. (a) Frequency response. Solid curve: fit to the absorption model; dashed curve: fit to a Lorentzian, (b) Time response. The curve is a fit to a single exponential growth model.

17

(a)

Absorption model fit parameters:
(Eq. (5))

$\alpha = 4.65(0.079)$ cm^{-1}
$\tau_0 = 0.734(0.018)$ msec

(b)

Fit parameters (Eq. (9)):

$C = 0.373(0.0002)$
$\tau = 3.06(0.015)$ msec

FIG 2.9. Temporal response of the GaAs:Cr sample. $1/e^2$ beam diameters: 6.0mm (pump) and 1.8mm (signal). Spatially averaged beam intensities are $I_{pump} = 172 \ mW/ \ cm^2$ and $I_{signal} = 2.4 \ mW/ \ cm^2$. (a) Frequency response. Solid curve: fit to the absorption model; dashed curve: fit to a Lorentzian, (b) Time response. The curve is a fit to a single exponential growth model.
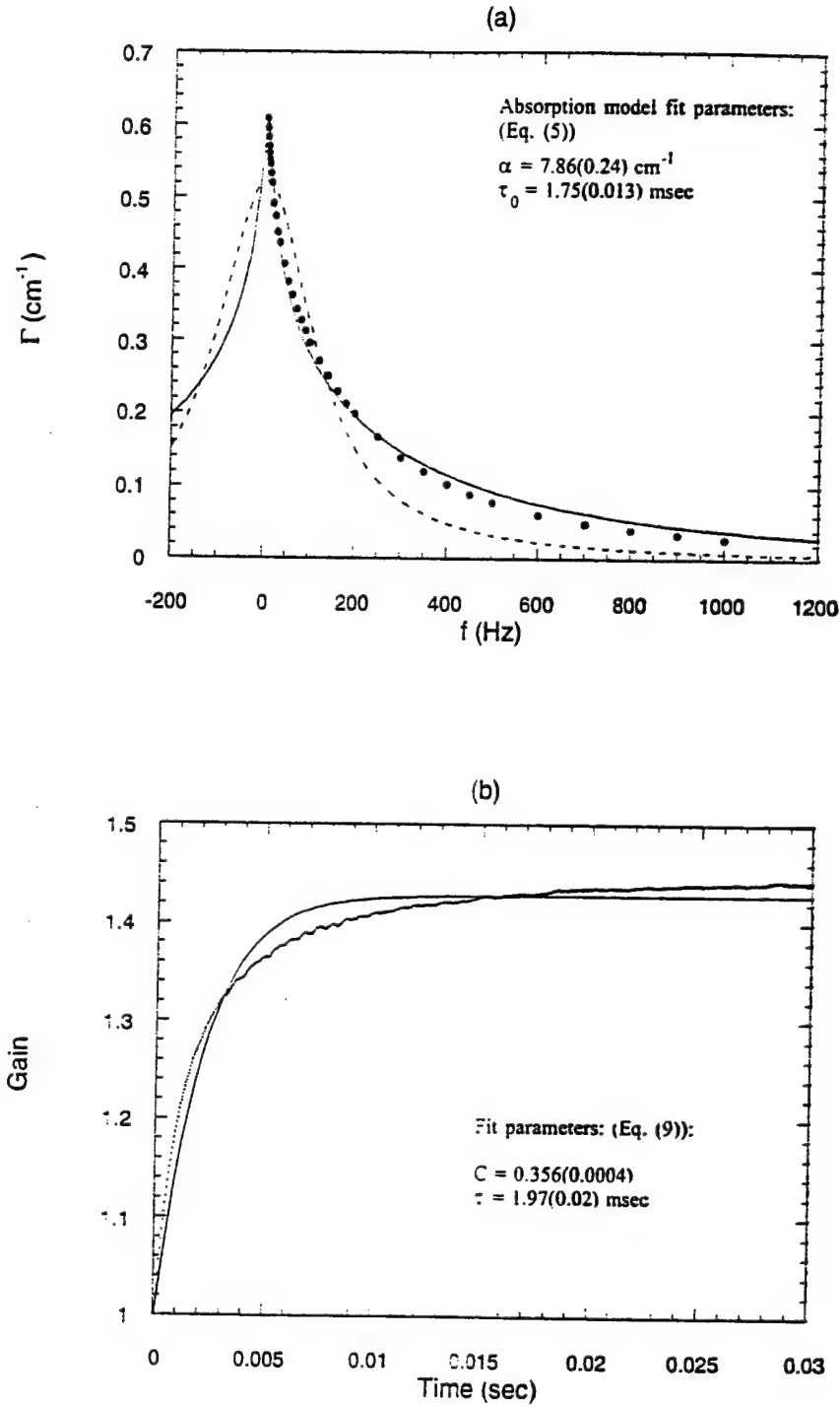
(a)

(b)
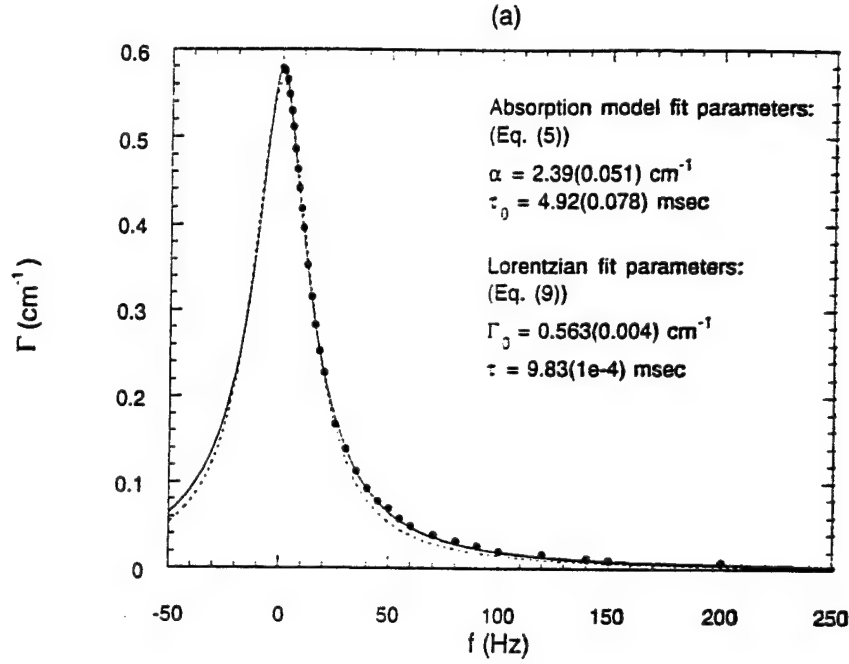
FIG 2.10. Temporal response of the GaAs:Cr sample. $1/e^2$ beam diameters: 10.7mm (pump) and 1.8mm (signal). Spatially averaged beam intensities are $I_{pump} = 54 \ mW/ \ cm^2$ and $I_{signal} = 2.4 \ mW/ \ cm^2$. (a) Frequency response. Solid curve: fit to the absorption model; dashed curve: fit to a Lorentzian, (b) Time response. The curve is a fit to a single exponential growth model.
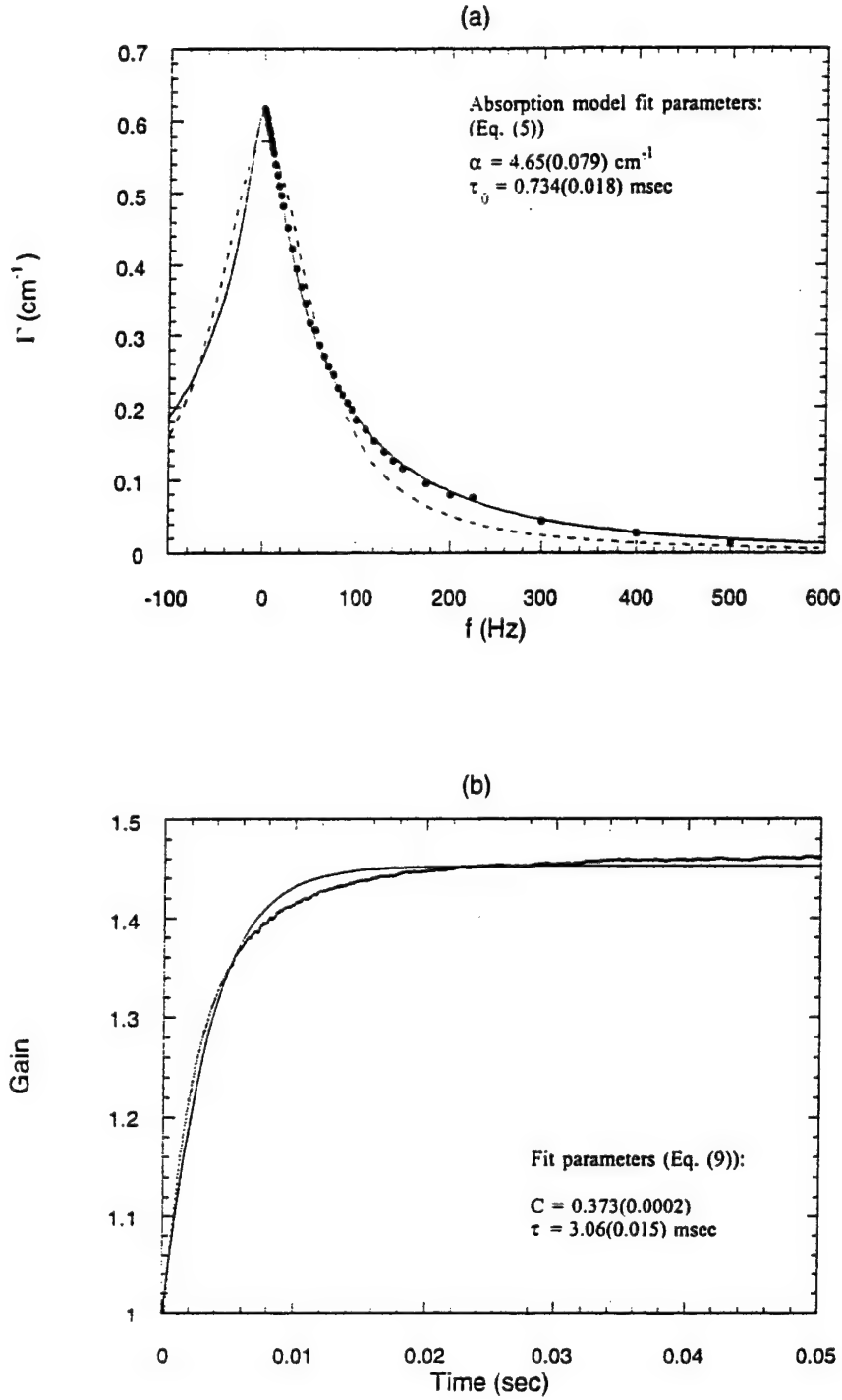
19
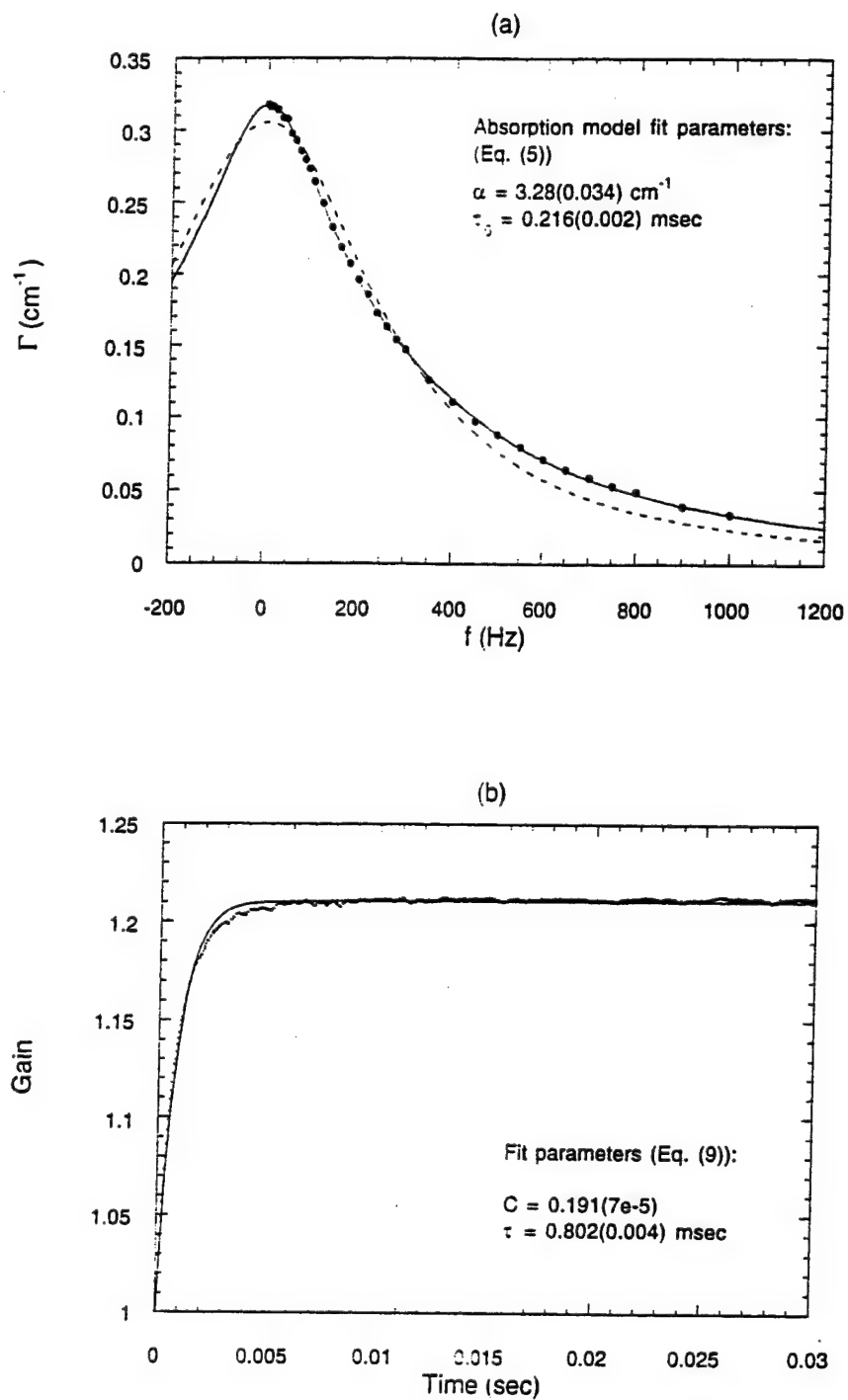
FIG 2.11. Temporal response of the GaAs:Cr sample in the presence of a flood beam. $1/e^2$ beam diameters: 2.0mm (pump) 1.8mm (signal), and 13.0mm (flood). Spatially averaged beam intensities are $I_{pump} = 1.55 \ W/\ cm^2$, $I_{signal} = 2.4 \ mW/\ cm^2$, and $I_{flood} = 142 \ mW/\ cm^2$. (a) Frequency response. Solid curve: fit to the absorption model; dashed curve: fit to a Lorentzian, (b) Time response. The curve is a fit to a single exponential growth model.
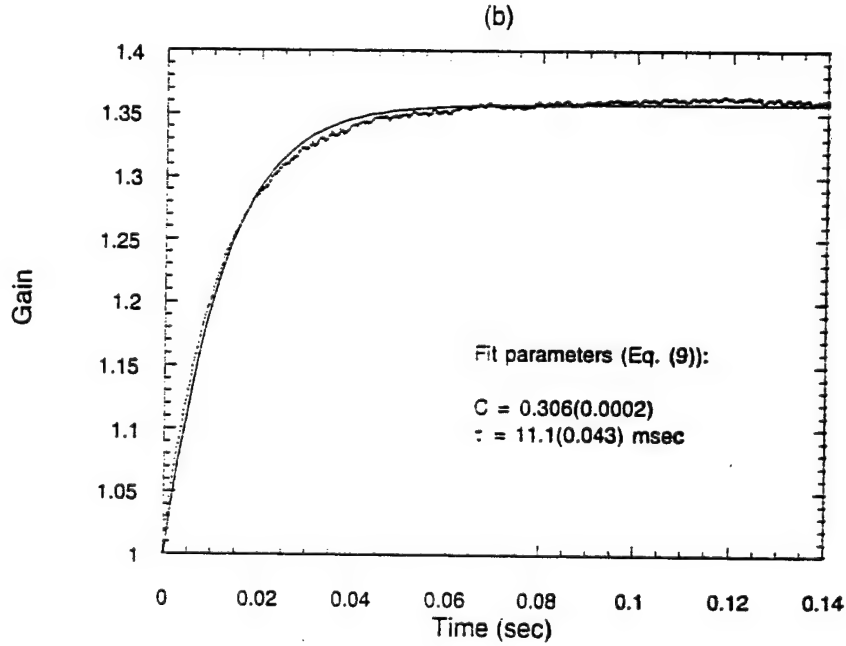
(a)

(b)
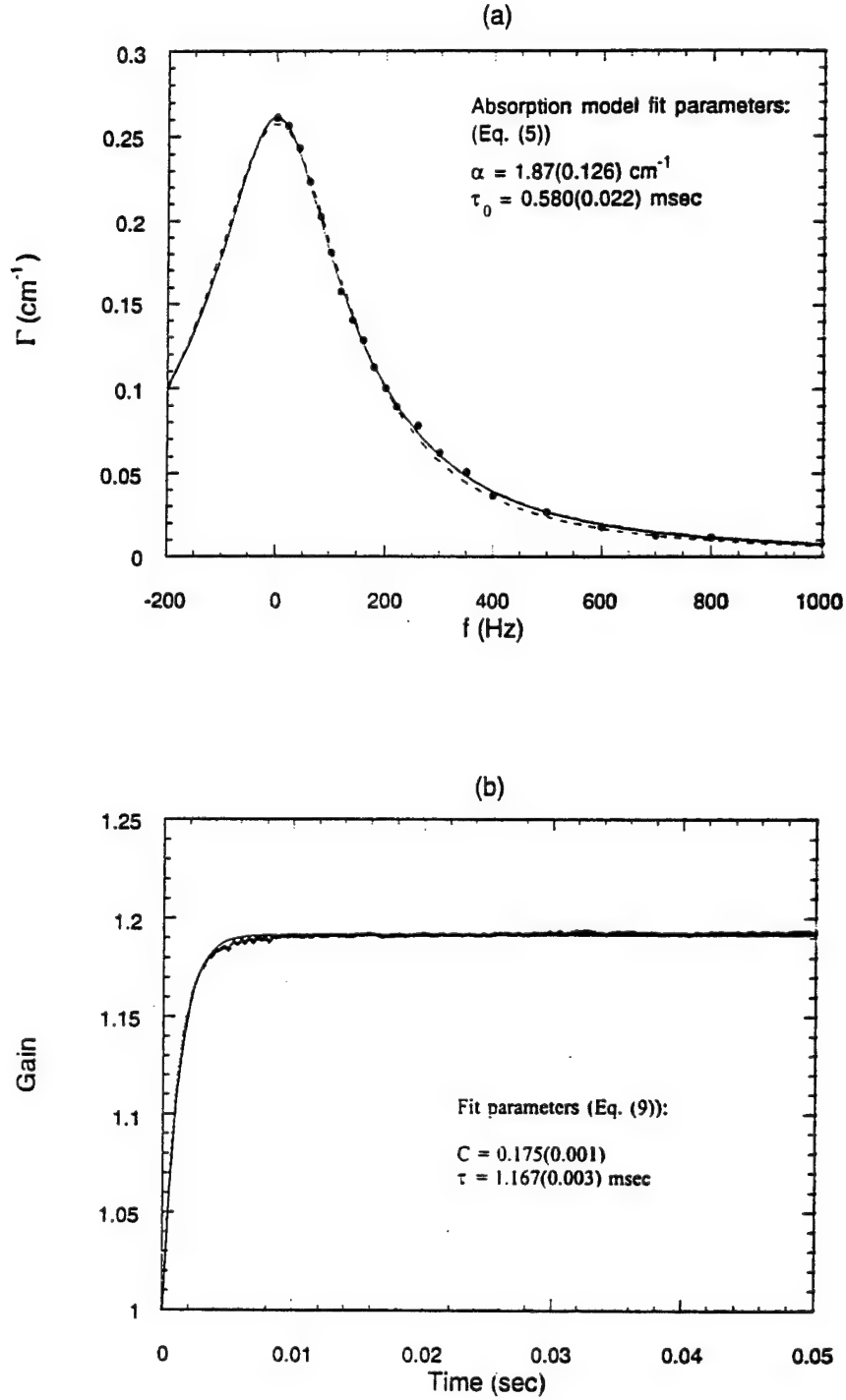
FIG 2.12. Temporal response of the GaAs:Cr sample in the presence of a flood beam. $1/e^2$ beam diameters: 6.0mm (pump), 1.8mm (signal), and 13.0mm (flood). Spatially averaged beam intensities are $I_{pump} = 172 \ mW/cm^2$, $I_{signal} = 2.4 \ mW/cm^2$ and $I_{flood} = 142 \ mW/cm^2$. (a) Frequency response. Solid curve: fit to the absorption model; dashed curve: fit to a Lorentzian, (b) Time response. The curve is a fit to a single exponential growth model.

(a)

Γ (cm⁻¹) vs f (Hz)

Absorption model fit parameters:
(Eq. (5))

$\alpha = 2.06(0.06)$ cm^{-1}
$\tau_0 = 2.01(0.04)$ msec

Lorentzian fit parameters:
(Eq. (2))

$\Gamma_0 = 0.224(0.001)$ cm^{-1}
$\tau = 3.67(0.04)$ msec

(b)

Gain vs Time (sec)

Fit parameters (Eq. (9)):

$C = 0.121(3e\text{-}5)$
$\tau = 4.42(0.01)$ msec

FIG 2.13. Temporal response of the GaAs:Cr sample in the presence of a flood beam. $1/e^2$ beam diameters: 10.7mm (pump) and 1.8mm (signal). Spatially averaged beam intensities are $I_{pump} = 54 \ mW/ \ cm^2$, $I_{signal} = 2.4 \ mW/ \ cm^2$ and $I_{flood} = 48 \ mW / cm^2$. (a) Frequency response. Solid curve: fit to the absorption model; dashed curve: fit to a Lorentzian, (b) Time response. The curve is a fit to a single exponential growth model.
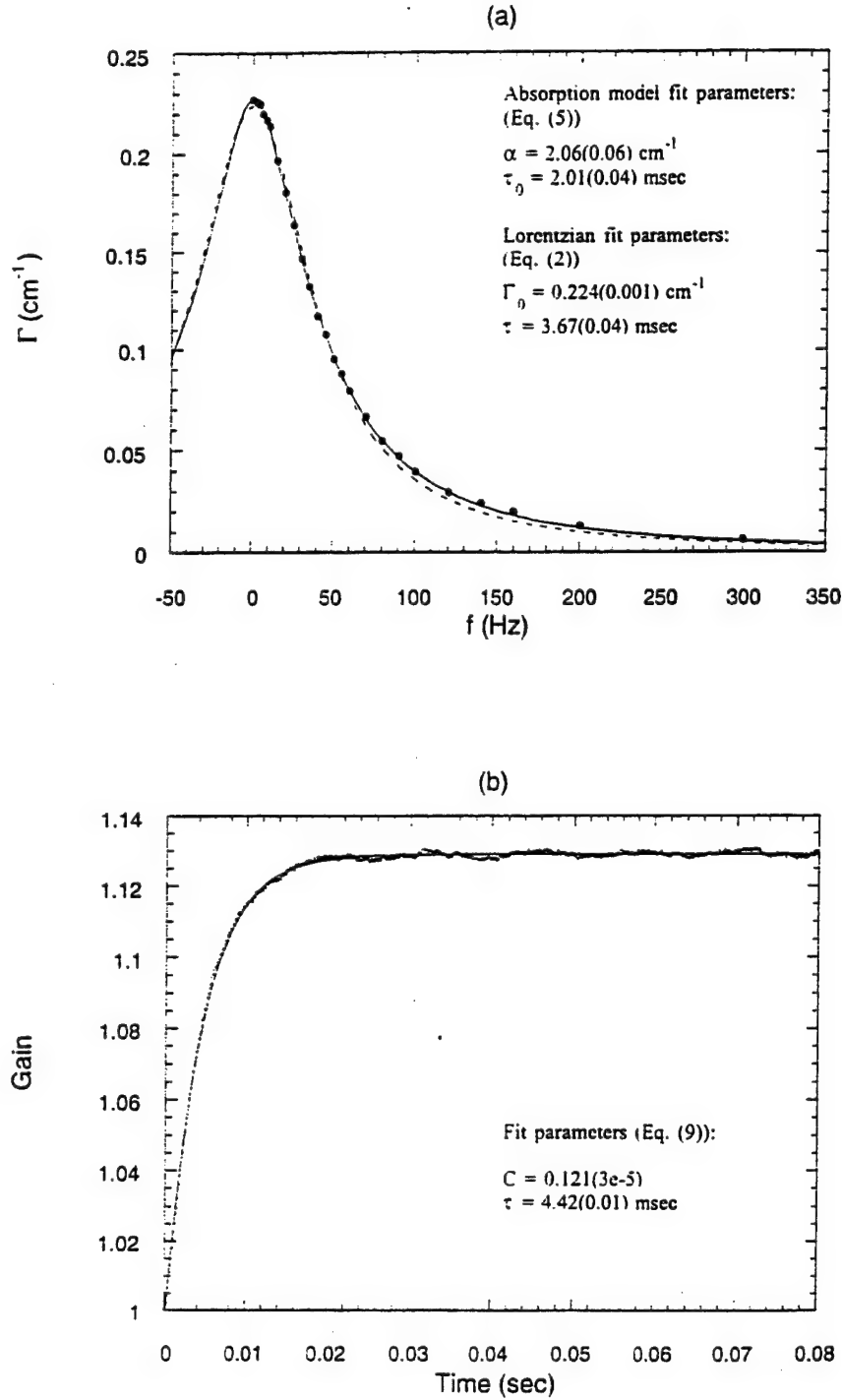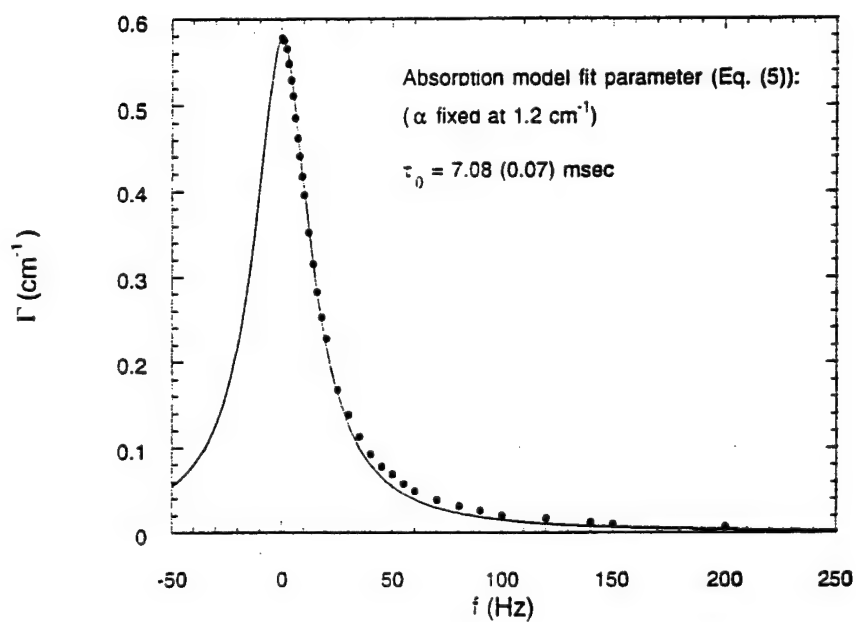
22

FIG 2.14. Fit of the data of Fig. 10(a) to the absorption model with the absorption coefficient parameter held constant at its known value of 1.2 cm^{-1}.

In Fig. 2.8, the Gaussian signal and pump beams have $1/e^2$ diameters of 1.8mm and 2.0mm, respectively. The data of Figs. 2.8(a) and 2.8(b), corresponding to the frequency and time response, respectively, were acquired under identical experimental conditions. Note that the beam diameters in this case are much smaller than the crystal thickness of 6.1mm. The dashed curve in Fig. 2.8(a) is an attempt to fit the data to the Lorentzian of Eq. (2) and it is apparent that the data depart significantly from this model. If the assumptions inherent in Eq. (2) were valid, the material time constant would be related to the full width at half maximum, Δ, of the Lorentzian by $\tau = 1 / \pi\Delta$.

The discrepancies between the data in Fig. 2.8 and the response expected from the simple theory can be attributed to the nonuniform intensity present inside the volume of the crystal occupied by the signal beam. As stated above, the sources of the nonuniformity in our case are the crystal absorption and the Gaussian beam profiles.

As shown in Section 2, in the case of plane wave beams the shape of the gain spectrum can be predicted using the known absorption coefficient of the material (see Eq. (2.5)). However, an attempt to fit the frequency response data of Fig. 2.8(a) to Eq. (5) yields a fitted value of the absorption coefficient that differs by a factor of more than six from the actual value of 1.2 cm^{-1}. This is due to the fact that the absorption model does not account for the Gaussian nature of the pump beam or the experimental geometry. The fit to Eq. (2.5) is therefore somewhat artificial, in the sense that the fitting parameters are not expected to match the actual values they are meant to represent. Since the effect of non-

24

plane-wave beams is always to reduce the frequency bandwidth, an attempt to fit the frequency response data to a model which neglects beam profiles always yields an absorption fitting parameter that equals or exceeds the actual absorption coefficient. This reflects the combined effects of the small Gaussian pump beam, the two-beam coupling geometry (including beam crossing angle and the crossing position of the beams in the crystal), and the crystal thickness.

The solid curve in Fig. 2.8(b) is a fit of the time response data to a single exponential rise:

$$\frac{I_{sig}(z = d/\cos\theta; \text{ pump on })}{I_{sig}(z = d/\cos\theta; \text{ pump off})} = e^{-\Gamma(t)d/\cos\theta} = \exp\left[C\left(1 - e^{-t/\tau}\right)\right] \qquad ,$$

2.9

where $I_{sig}(z = d/\cos\theta; \text{ pump on})$ is the signal beam intensity with the pump beam present, $I_{sig}(z = d/\cos\theta; \text{ pump off})$ is the signal beam intensity with no pump beam, the signal beam is assumed to propagate in the z-direction, C is a constant that determines the steady-state gain, d is the crystal thickness, and θ is beam crossing half-angle. Not surprisingly, these data show a correspondingly large deviation from the simple time response model and the fit to Eq. (2.9) yields fitting parameters that do not reflect the actual time response of the system, as it is not single exponential.

The effect on the temporal response of increasing the diameter of the Gaussian pump beam is shown in Figs. 2.9 and 2.10, in which the pump beam $1/e^2$ diameters have been

increased to 6.0mm and 10.7mm, respectively. The signal beam diameter remains at 1.8mm. Notice that the quality of the fit in Figs. 9(a) and 10(a) to the pure absorption model (solid curves; Eq. (2.5)) is extremely good, even though the fitted absorption parameters still deviate from the actual value of the absorption coefficient by factors of 3.9 and 2.0, respectively. As expected, the time domain data in Figs. 2.9(b) and 2.10(b) show a deviation from single exponential response.

In our experiment, we had insufficient laser power to simultaneously achieve a plane wave pump beam and a large pump-signal intensity ratio. These conditions would have allowed us to extract an accurate material time constant from a fit of the frequency response data to the absorption model. Because of this experimental limitation, we took an alternative approach which consisted of illuminating the crystal incoherently from the exit face side with a large diameter beam at the same wavelength as the pump and signal beams, obtained from a separate laser. If the intensity and diameter of this "flood beam" is chosen appropriately, the effect is to significantly reduce the intensity variations in the crystal due to all sources. To the degree that intensity uniformity is accomplished, the frequency response should take on the Lorentzian shape of the zero-absorption, plane wave theory of Eqs. (2.1) and (2.2).

Figures 2.11 - 2.13 show frequency and time response data with a flood beam illuminating the crystal from the exit face side. Except for the addition of flood light, the conditions for the data of Figs. 2.11 - 2.13 were identical to those in Figs. 2.8 -2.10, respectively. If we compare Figs. 2.11(a) and 2.8(a), for both of which the pump beam is

at its smallest diameter (2.0mm), we see that the addition of the flood light in Fig. 2.11(a) has caused the frequency response to approach Lorentzian behavior. The remaining discrepancy is due to the fact that the pump beam intensity is more than ten times that of the flood in this case and so the flood beam is unable to completely compensate for the intensity nonuniformity in the crystal. In Fig. 2.12, the pump and flood beams are similar in intensity and the pump beam diameter has been increased relative to Fig. 2.11, to 6.0mm. In this case, the frequency response data come quite close to fitting a Lorentzian function, an indication that the intensity distribution in the crystal is approaching uniformity. This is also apparent in the corresponding time response data in Fig. 2.12(b).

The greatest intensity uniformity was achieved with the largest pump beam diameter, 10.7mm, and with the flood light illuminating the crystal, the flood and pump beam intensities being approximately equal. These data are shown in Fig. 2.13 and from the Lorentzian and single exponential fits in Figs. 2.13(a) and (b) come our best estimate of the material time constant for this GaAs sample. The time constants obtained from the frequency and time domain data in Fig. 2.13 are in close, but not perfect agreement. This is due to the small amount of remaining intensity nonuniformity in the crystal, which is evident from the small deviation of the frequency response data from Lorentzian behavior. Note that it is impossible to completely compensate for material absorption and non-uniform beam profiles using a flood beam. However, the goodness of the fits in Figs. 2.13(a) and (b) and the close agreement of the time constants obtained from the frequency and time domain data (3.67(0.04) msec and 4.42(0.01) msec, respectively, at

an approximate total intensity of 52 mW/cm^2) indicate that a high degree of intensity uniformity has been achieved.

It was mentioned above that the absorption model fit of the frequency response data in Fig. 2.10(a), corresponding to the 10.7mm pump beam and no flood beam, yields an absorption coefficient of 2.4 cm^{-1}, which is twice the actual value. The fitted time constant also differs from the expected value based on the results in Fig 2.13 and assuming a linear intensity dependence. Nevertheless, the quality of the fit to the absorption model in Fig 2.10(a) is very good. The ability of the absorption model to fit the frequency response data well in almost all cases while yielding unphysical values of the absorption coefficient and time constant, is due in part to fact that the position dependent illumination, whether it originates from absorption or Gaussian beam profile, decreases the bandwidth. Thus a large absorption coefficient compensates for the beam profile effects. The other factor is the compensating relationship between the two fitting parameters. Increasing (decreasing) the value of the absorption parameter leads to a narrowing (broadening) of the gain bandwidth, while a change in the time constant parameter has the opposite effect. There is, then, a wide range of parameter pairs that yield a reasonable fit to the data. Since the absorption coefficient of the GaAs sample is known, we have also fit the data of Fig. 2.10(a) to the absorption model with the absorption parameter fixed at its known value of 1.2 cm^{-1}. This fit is shown in Fig. 2.14 and the resulting fitted time constant is 7.08(0.07) msec. For comparison, the predicted value of this time constant, based on linear intensity dependence, is 6.8 msec. This is evidence that for this pump beam diameter, 10.7 mm, and the absence of a flood beam,

the influence of the Gaussian nature of the pump beam on the photorefractive temporal response has been largely eliminated.

We have observed similar two-beam coupling gain spectrum narrowing effects in four other photorefractive semiconductors: ZnTe:Mn:V, CdMnTe:V, CdTe:Ge, and CdTe:V.

2.4. CONCLUSIONS

In this section, we have illustrated the influence of bulk absorption, beam profiles, and experimental geometry on measurements of photorefractive temporal response, in the undepleted pump case and in the limit of small coupling. These effects act to narrow the bandwidth and to cause the spectra to deviate from the expected Lorentzian shape.

We have shown that if accurate values of the photorefractive material time constant are to be obtained, spatial variations of total laser intensity in the crystal must either be eliminated or accounted for in the model used to extract the temporal parameters. If enough laser power is available, the pump beam can be expanded to closely approximate a plane wave. In this case, the absorption model (Eq. (2.5)) should describe the frequency response and a fit to this model would yield the material time constant. As we have shown, an alternative method is to achieve an approximately uniform volume intensity distribution by incoherently illuminating the material with a uniform intensity beam. Another method, in principle, is to use a very thin sample. However, in addition to depending on the availability of a thin sample having similar characteristics to the one

being used in an actual system, the overall gain in this case may not be sufficient to make

accurate measurements.

3 ENHANCEMENT OF BEAM COUPLING IN TIN HYPOTHIODIPHOSPHATE

3.1 INTRODUCTION

Tin hypothiodiphosphate ($Sn_2P_2S_6$, SPS) was shown to be a promising photorefractive material for the near-infrared region of spectrum with a relatively high transient gain factor (up to $10 cm^{-1}$) and rather short response time of the transient peak (10^{-1} to 10^{-2} s) [12-15]. SPS is a monoclinic ferroelectric crystal which belongs to the P_c symmetry class [13,14]. The photorefractive grating recording via diffusive charge transport was reported for this material at $\lambda = 0.6328$ μm [12,13]. The virgin crystals are also sensitive in the near infrared ($\lambda = 1.06$ μm) but exhibit much smaller beam coupling gain than with red light. [14,15]. The sensitivity to near infrared light can be improved considerably by pre-illumination of the sample with light. The detailed description of the model of photorefractive recording in SPS is given in refs. 14 and 15.

According to this model, two kinds of movable charges are responsible for the formation of stationary photorefractive gratings under CW illumination. At first, the "fast" grating is built up by the redistribution of photoexcited carriers (presumably electrons). The "slow" grating develops due to the redistribution of thermally excited carriers (holes), which partially compensate the initial grating. As a consequence, the steady-state gain factor, which is established after approximately 10^3 s, is much smaller than the peak gain factor.

By using the moving grating technique, without an applied electric field, it is possible to significantly increase the steady-state two-beam coupling gain in photorefractive $Sn_2P_2S_6$. Another technique of gain enhancement consists of cooling of the sample to -

30°C. The measured data confirm the existence of two out-of-phase gratings in $Sn_2P_2S_6$ generated by charge carriers of different sign, with relaxation times of 70 ms and 500 s. With small frequency detuning of one of two writing beams, the steady-state gain can be achieved close to the peak value of the transient gain for strict frequency degeneracy. also discuss another way to increase the steady-state gain, which consists of decreasing the SPS sample temperature.

3.2 Experiment

In our experiments the single-mode, single-frequency 1.06 μm radiation of a diode-pumped Nd [3+]:YAG laser is used for the grating recording. A beam splitter forms two beams, with the strong pump beam passing through an electro-optic modulator. The two light beams are directed to the SPS sample in the plane normal to the OY axis in such a way that the grating vector is parallel to the OX axis.[16] The electro-optic modulator is driven with a periodic saw-tooth signal. The amplitude of modulation is adjusted to provide exactly a 2π phase shift in the pump wave during one period. In this way, linear-in-time modulation of phase is introduced in the pump wave, which is equivalent to a frequency shift of the pump wave with respect to the signal wave. The intensities of the pump and signal beams on the input face of the sample were 15 W/cm^2 and 43 mW/cm^2, respectively.

The crystals of $Sn_2P_2S_6$ studied in this work were grown in the Institute of Solid State Physics and Chemistry, Uzhgorod State University, 294000 Uzhgorod, Ukraine. Typical sample sizes are 5x5x1.2 mm^3 along X, Y, and Z axes. To increase the sensitivity of the crystal to infrared light it was illuminated by incoherent white light

(100W- halogen lamp at 5 cm distance from the sample, exposure time 30 min). Once illuminated, the sample remains sensitive for a minimum of one day. Consecutive write-erase cycles with infrared light do not change, in first approximation, the sensitivity to subsequent recording.

With this set-up we measure first the dynamics of the beam coupling for the strictly degenerate case at ambient temperature 20°C (Fig. 3.1, top graph). The results agree qualitatively with that reported in [16]. When the pump beam is switched on, the intensity of the weak signal beam increases quickly, reaching a certain peak value, and then decreases with a much slower rate. The steady state is established after 10^3 seconds. This type of dynamics suggested the model of two movable species of charge carriers, with simultaneous excitation resulting in partial compensation of a grating in steady-state (see, e.g., Ref.18). The lack of dependence of the slow response time on light intensity leads to the conclusion that the slow grating is formed by thermally excited carriers [14,15].

One can expect that the recording of this slow grating can be eliminated by proper choice of frequency shift in the moving grating technique. If the frequency detuning is larger than the reciprocal relaxation time for the slow component, but still much smaller than that for the fast component, it should be possible to reach the steady-state gain factor close to its transient peak value in the frequency degenerate case. For diffusion dominated charge transport the result must be insensitive to the direction of grating motion. A second advantage is the considerable reduction of the relaxation time of the signal amplification.
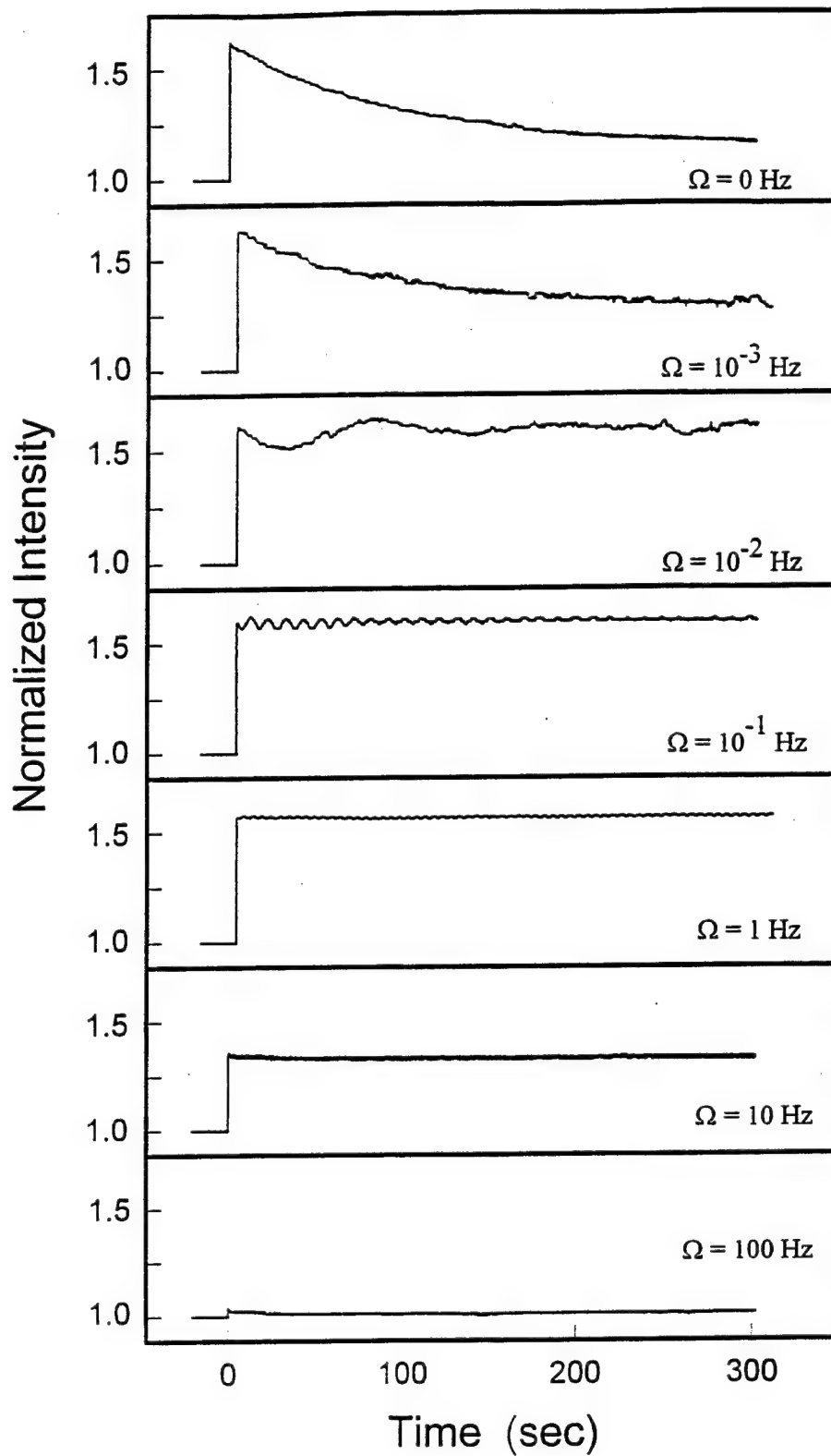
Fig. 3.1   Dynamics of the signal beam intensity in beam-coupling experiment for

different values of frequency detuning.

Fig. 3.1 shows the temporal variation of the signal beam intensity for different values of frequency detuning Ω. It is quite clear from these data that for Ω less than 1Hz the peak value of gain is the same for all these curves while the steady-state value of gain is gradually increasing when Ω becomes larger. This is in complete agreement with our expectations. For large frequency detuning the transient peak is no longer visible, but the saturation value of gain becomes smaller than at low frequencies. This decrease of intensity is a consequence of the grating moving too fast compared to $1/\tau_f K$, where τ_f is the relaxation time of the fast component and K is the spatial frequency of the grating.

We measured the dependence of the gain factor on frequency detuning (Fig.3.2). The gain factor Γ is introduced in the usual way as $\Gamma = (1/d)\ln[I_s/I_s^o]$, where d is the sample thickness, I_s and I_s^o are the intensities of the output signal wave in presence and with no pump wave, respectively. Two values are given for any particular frequency detuning Ω , one for transient gain (I_s stands for the peak value of intensity after onset of the pump wave) and other for steady-state gain (I_s stands for saturated value of weak beam intensity). The logarithmic scale is chosen for Ω to clearly show the frequency dependence of the steady state gain at low modulation frequencies. This kind of plot does not permit showing the response for negative values of frequency detuning. It should be emphasized, however, that within experimental error the measured values for $+\Omega$ and $-\Omega$ are the same.
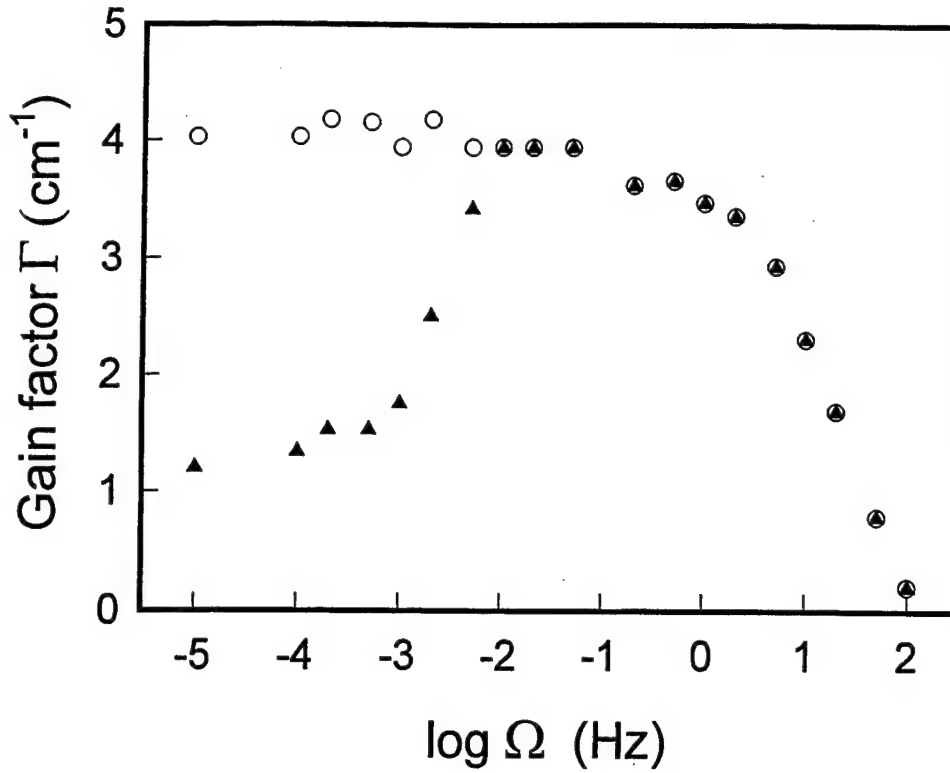
Fig. 3.2 Frequency detuning dependence of the gain factor. Open dots represent the transient gain, filled dots represent the steady-state gain.

It is clear from Fig. 3.2 that with the pump intensity of 15 W/cm^2 one can use SPS within the range of frequency detuning (0.005 to 1Hz) with loss of gain of no more than 15 %. The characteristic relaxation times (estimated from frequency detuning necessary to change the ultimate gain factor two times) are $\tau_f = 70$ ms and $\tau_s = 500$ s for fast and slow components, respectively.

As can be seen from Fig. 3.1, the intensity of the amplified signal beam is periodically modulated with a frequency equal to that of the frequency detuning, Ω. Figure 3.3 represents the dependence of deviation from the mean value of gain factor

as a function of frequency detuning. For the worst situation, at $\Omega = 0.005$ Hz the largest deviation $\Delta\Gamma/\Gamma$ does not exceed 0.17. Note that even in this case the mean value of Γ is established within 100 ms, which is much faster then the steady-state gain for beams with the same frequency.
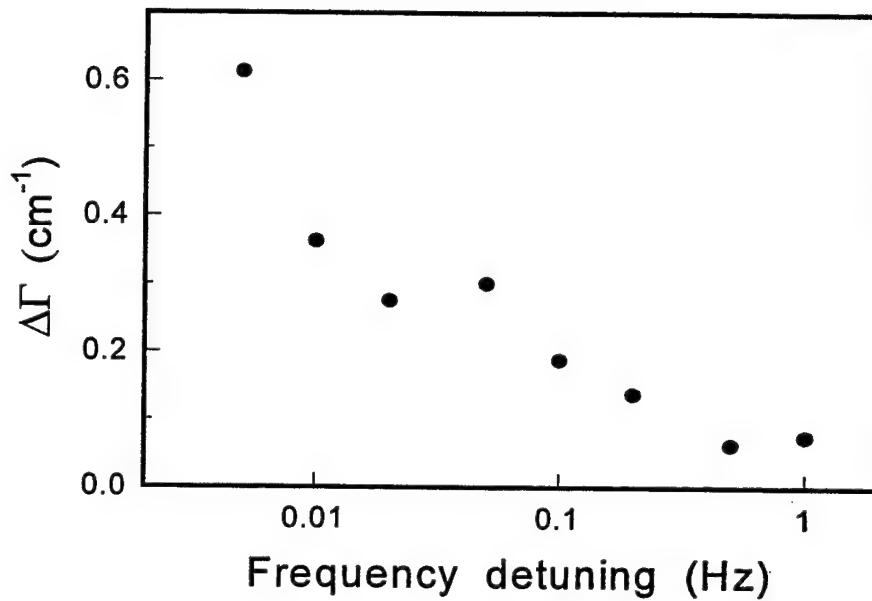

Fig. 3.3 Amplitude of temporal variations of the gain factor versus frequency detuning.

Since the slow component is connected to thermally excited carriers it must be sensitive to variation of temperature. It is reasonable to expect a considerable increase in the relaxation time for the slow component τ_s when decreasing the temperature of the sample.

The sample was mounted on the cold finger of a Peltier microcooler and measured the dynamics of the beam coupling with the reduced temperature. Fig. 3.4 shows our preliminary results. It can be clearly seen that for the reduced temperatures (*i*) the peak value of intensity becomes larger and (*ii*) the relaxation time for slow component τ_s becomes longer. Assuming the usual exponential temperature dependence for thermal excitation rate, $w \propto \exp(-\Delta E/kT)$, we can get an upper limit for characteristic energy of thermal excitation of carriers, $\Delta E \geq 0.4$ eV. Here k is the Boltzmann constant and T is the absolute temperature. Cooling the sample to -30°C increased the steady-state gain by a factor of five over that at room temperature.
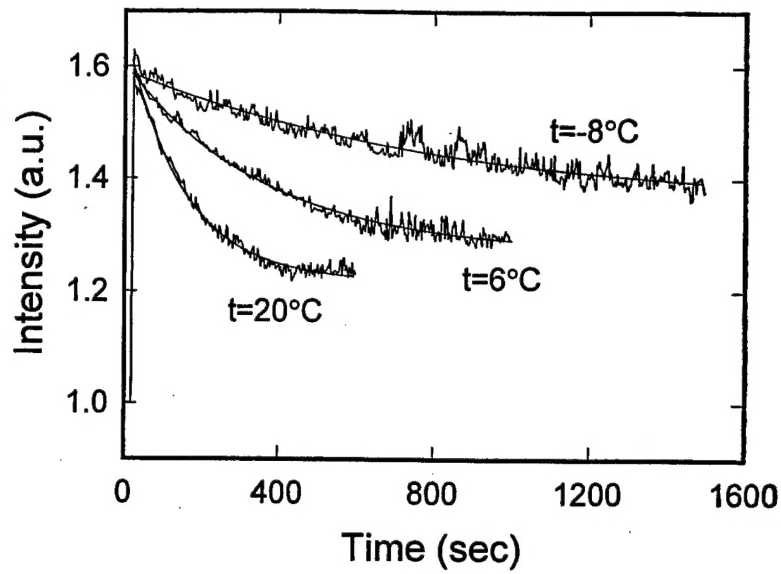
Fig. 3.4 Dynamics of the signal beam intensity in beam-coupling experiment for three consecutive measurements with gradual decrease of temperature, starting from room temperature. The lines show an exponential fit to the experimental data.

3.3 SUMMARY

To summarize, both experiments validate the model formulated in Ref. 1 in which the inhibition of the beam coupling is attributed to formation of an out-of-phase grating by thermally excited charge carriers. Both techniques proposed provide considerable increase of the steady-state gain with no applied electric field, which is important from the practical point of view.

4 REFERENCES

1. B. I. Sturman, "Interaction of two light waves in a crystal caused by photoelectron diffusion and drift", Sov. Phys. Tech. Phys., **23**, 589 (1978).o

2. P. Yeh, *Introduction to Photorefractive Nonlinear Optics* (Wiley, New York, 1993).

3. L. Dai, C. Gu, and P. Yeh, " Effect of position-dependent time constant on photorefractive two-wave mixing", J. Opt. Soc. Am. B, **5**, 1693 (1992).

4. Ph. Delaye, L.A. De Montmorillon, an G. Roosen, "Transmission of time modulated optical signals through an absorbing photorefractive crystal", Opt. Commun. **118**, 154 (1995).

5. A. Hermanns, C. Benkert, D.M. Lininger, and D.A. Anderson, IEEE J. Quant. Electron. **28**, 750 (1992).

6. D. Fluck, S. Brulisauer, and P. Gunter, " Photorefractive two-wave mixing with focused Gaussian beams", Optics Commun., **115**, 626 (1995).

7. L. Boutsikaris and F. Davidson, Appl. " Two-wave mising of time varying non-plane wave optical fields in photorefractive materials", Opt. **32**, 1559 (1993).

8. L. Solymar, D.J. Webb, and A. Grunnet-Jepsen, " Forward wave interactions in photorefractive materials", Prog. Quant. Electr., **18**, 377 (1994).

9. F. Vachss," An analytical expression for the photorefractive two beam coupling response time", in Tech. Digest, Photorefractive Materials, Effects, and Devices, p140, Aussois (France) 1990.

10. G. Brost, "Numerical analysis of photorefractive grating formation dynamics at large modulation in BSO", Opt. Commun., **96**, 113 (1993). (Note that the analysis presented here is for an applied field, but for m =1 the results for no applied field are similar)

11. S. Odoulov, A. Shumelyuk, G. Brost, and K. Magde, "Enhancement of beam coupling in the near infrared for tin hypothiodiphosphate", Appl. Phys Lett. **69,** 3665 (1996).

12. A. A. Grabar, R. I. Muzhikash, A.D. Kostiuk, and Yu. M. Vysochanskii, Sov. Physics, Solid State, **33,** 1314-1316 (1991).

13. A. A. Grabar, Yu. M. Vysochanskii, I. M. Stoyka, M. M. Dan'ko, and V. Yu. Slivka, Ukrainian Physical Journal, **39,** 941-942 (1994).

14. A. Shumelyuk, U. Hellwig, R. Rupp, S. Odoulov, and A. Grabar, Opt. Lett., **21,** 752-754 (1996).

15. A. Shumelyuk, U. Hellwig, R. Rupp, S. Odoulov, and A. Grabar, accepted for publication in JOSA B.

16. We adopt and use the following notations for crystal axes [3]: axis OY is normal to the unique plane of symmetry of the crystal, axis OX is nearly parallel to the axis of spontaneous polarization.

17. S. Zivkova and M. Miteva, J. Appl. Phys. **68,** 3099-3103 (1990).